

Caecilia Charbonnier · Lazhari Assassi · Pascal Volino · Nadia Magnenat-Thalmann

## Motion study of the hip joint in extreme postures

**Abstract** Many causes can be at the origin of hip osteoarthritis (e.g., cam/ pincer impingements), but the exact pathogenesis for idiopathic osteoarthritis has not yet been clearly delineated. The aim of the present work is to analyze the consequences of repetitive extreme hip motion on the labrum cartilage. Our hypothesis is that extreme movements can induce excessive labral deformations and lead to early arthritis. To verify this hypothesis, an optical motion capture system is used to estimate the kinematics of patient-specific hip joint, while soft tissue artifacts are reduced with an effective correction method. Subsequently, a physical simulation system is used during motion to compute accurate labral deformations and to assess the global pressure of the labrum, as well as any local pressure excess that may be physiologically damageable. Results show that peak contact pressures occur at extreme hip flexion/ abduction and that the pressure distribution corresponds with radiologically observed damage zones in the labrum.

**Keywords** Motion capture · Physically-based simulation · Extreme motion · Hip osteoarthritis

### 1 Introduction

Osteoarthritis (OA) affects the hip joint and is a common problem for many people. This pathogenesis can be caused by femoroacetabular impingements (FAI) that occur when there is an abnormal contact between the proximal femur and the acetabular rim [13]. Generally, two basic mechanisms of impingement can be distinguished (Fig. 1): the cam FAI caused by a non-spherical femoral head and the pincer FAI due to acetabular overcover. These morphological abnormalities induce degenerative lesions of the cartilages and

more specifically, lesions of the superior labrum [31].

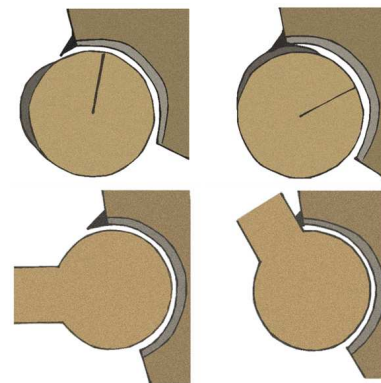


**Fig. 1** Top: Reduced head-neck offset of cam FAI: non-spherical head abuts the acetabular rim. Down: Excessive overcoverage of the femoral head by acetabulum in pincer FAI, causing abutment against the acetabular rim.

Although the mechanism of degeneration in the cam/ pincer -FAI hip is well understood, the exact pathogenesis for idiopathic OA has not yet been clearly delineated. Indeed, changes in the movement and alignment of the hip (e.g., subluxation) can be other potential causes of early OA [24]. Therefore, do people practicing a sport requiring extreme movements present a higher risk of developing arthritis? To detect arthrogenous activities, a clinical study with 30 professional ballet dancers is being conducted. The aim of this study is to verify if repetitive extreme motion could be a factor of joint degeneration through excessive labral deformations.

To pursue this goal, an optical motion capture system is used to obtain bone poses of patient-specific hip joint 3D models, reconstructed from magnetic resonance imaging (MRI) data. The major drawback with this system is the soft tissue deformation due to muscle contractions, causing markers movements with respect to the underlying bones. To solve this issue, we propose a correction method combining nonlin-

C. Charbonnier  
MIRALab, University of Geneva  
7, rte de Drize  
CH-1227 Carouge  
Switzerland  
Tel.: +41-22-3791122  
Fax: +41-22-3790079  
E-mail: charbonnier@miralab.unige.ch

ear optimization and joint motion constraints, and allowing some shifts at the joint. The estimation of the hip kinematics was successfully validated with data collected from a dynamic MRI protocol.

Subsequently, a fast functional joint model is used to simulate the mechanical behavior of the soft tissues during motion. To this end, we have developed a physical simulation system that aims at computing accurately the deformations of the cartilage during the joint motion, estimated from the optical capture system. The goal is to compute precisely the strain and stress, in order to assess the global pressure of the labrum, as well as any local pressure excess that may be physiologically damageable.

Finally, simulation results are presented for one dancer and for various extreme dancing movements, and are compared with the radiological analysis of patient's MR images. Moreover, a morphological analysis is performed using standard measurements (e.g., femoral alpha neck angle, acetabular depth and version), typically used to diagnose cam/ pincer -FAI. Since our hypothesis is that the hip OA is not only the result of cam/ pincer -FAI, the prevalence of the subject's hip joint must be evaluated, in order to confirm that repetitive extreme motion may lead to labral microtrauma.

## 2 Related works

To derive the motion of the skeleton, various methods with direct access to the bone (e.g. intra-cortical pins [5], external fixators [8], percutaneous trackers [29]) have been proposed. These techniques are robust, but are strongly invasive. Therefore, the optical motion capture system appears as a non-invasive solution for studying the kinematics of the joint, allowing the recording of a large range of motion. However, the internal bone remains inaccessible and the resulting estimations are embedded with soft tissue artifacts (STA). Displacements of individual markers of more than 20 mm are observed [8] and the STA associated with the thigh is greater than any lower limb segment.

Several methods were proposed to reduce these errors, but these techniques have the following limitations: 1) A recent study [9] has showed that some mathematical approaches [2] are unstable and do not perform better than traditional bone pose estimators (e.g., SVD algorithm [36]). These approaches are thus not efficient to compensate STA 2) Some methods [7,26] are based on invalid assumptions (e.g., considering that the skin moves linearly between two postures) 3) Some techniques [25] are limited to the use of ball and socket joints (i.e., meaning that no shifts are allowed), which simplifies the joint structures and is not subject-specific.

To overcome this issue, we propose to extend previous works with a correction method combining nonlinear optimization (i.e., we use a quadratic algorithm for robustness and fast convergence) to optimize joint center locations and segment orientations, and joint constraints to avoid non-physiological joint translation and even dislocation, but allowing some shifts at the joint.

Once the femoroacetabular movements are precisely estimated, they provide the motion input for the physically-based simulation. The analysis of the stress and contact distribution in the acetabulum region was the focus of several studies, based on either Mass-Spring systems [22,27] or Finite-Element methods (FEM) [1,34]. Normal and pathological hip joints (e.g., dysplastic hip [34], cam/ pincer -FAI hip [10]) were also intensively investigated.

However, these studies do not generally simulate complex geometrical 3D meshes (for instance patient-specific models) during sophisticated movements. Indeed, the movement is typically simplified to simple anatomical angles or to low amplitude motion. Therefore, we believe that the combination of physical simulation and motion capture can be an effective approach to study the hip joint in extreme postures.

## 3 Material and methods

Our study is conducted with professional female ballet dancers. The institutional medical-ethical committee approved the study and the subjects gave written informed consent. For each dancer, patient-specific 3D models (1 femur, 1 hip bone, 1 labrum and 1 skin) of the hip joint were reconstructed from a static MRI protocol [15]. The same bone models were used to evaluate the hip joint center's (HJC) position using a functional method, detailed in [14]. The pelvis and femoral coordinates' systems were implemented following the recommendations of the International Society of Biomechanics [37].

The acetabular region represents the contact area. Since our goal is to assess the labral deformations during extreme movements, only the labrum was tetrahedralized ( $\sim 4$  K tetrahedra), whereas the 3D models of the bones were hypothesized as rigid bodies. A method based on the medial axis information was used to construct the corresponding tetrahedral mesh, as depicted in [3].

### 3.1 Motion recordings

Two clusters of six 7 mm spherical markers were affixed onto the lateral and frontal parts of both thighs. Six markers were also stuck on the pelvis (Fig. 2a). These skin markers were arranged to ensure their visibility to the cameras throughout the range of motion. Additional reflective markers were distributed over the body to confer a more complete visualization from general to detailed.

Data from the subjects were acquired during 3 different dancing activities: grand plié, frontal split and développ    la seconde (Fig. 2b,c,d). These movements have been chosen, because they require extreme hip flexion and/ or abduction. Moreover, they seem to create significant stress in the hip joint, according to some dancer's pain feedback. The markers trajectories were tracked within a 45.3 m<sup>3</sup> measurement volume (3.6 x 4.2 x 3 m) using 8 infrared cameras (Vicon MX 13i, Oxford Metrics, UK), sampling at 120 Hz.

### 3.2 Subject calibration

Before converting markers trajectories into animation, the skin markers must be replaced into the MRI space to establish a correspondence between the markers set-up and the segmented 3D models. To establish the required calibration, our idea is to combine MRI and 3D body scan information to have an accurate approximation due to marker positions on the skin.

Following the motion recordings, the subjects underwent a 3D body scan (Vitus Pro, Vitronic, Germany) with the markers still in place to retrieve their exact external body surface. The positions of the skin markers were identified on the resulting body scan mesh using a least-squares sphere fitting technique [35]. Finally, the body scan mesh was registered [28] with the skin generated from MR images, performing the required calibration (Fig. 2a).

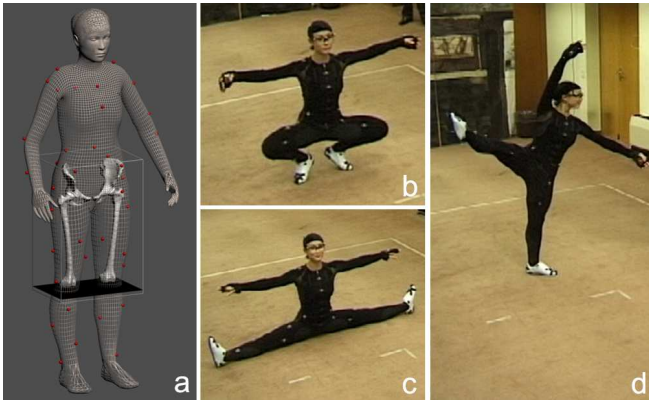


**Fig. 2** a) Calibrated subject showing the markers configuration with the reconstructed hip joints, the MRI volume and the body scan mesh (the segmented skin is not shown for clarity) b,c,d) Dancing movements recorded with the Vicon system: grand plié (b), frontal split (c) and développée à la seconde (d).

### 3.3 Bone poses estimation

Rigid motion of the bone segment cannot be robustly estimated from the markers trajectories, unless the STA is small. To reduce STA, our correction method works in 2 phases: 1) First, we combine nonlinear optimization and joint constraints. The optimization provides us for each segment with the rotation and translation that minimize the error made globally on all the markers, while the HJC remains fixed during this first phase 2) Although the HJC can be considered as fixed during low amplitude movements, this is not true for extreme motion. Indeed, a potential subluxation may occur to avoid bones penetration. Thus, our algorithm adjusts the HJC by detecting collisions among the articular bones, the goal being to reach the non-penetrating state. More details about these 2 phases are given below:

*Phase 1:* During a movement, several components contribute to the motion of a skin marker. Assuming that the pelvis motion is known, the HJC can slightly move during the rotation of the thigh. This introduces one translation  $T_c$  and one rotation  $R$ . Additionally, a rigid displacement is observed due to STA which is denoted by another translation  $T_s$ . The motion of a marker with respect to the pelvis can hence be described by 3 transformations successively applied. Since we cannot accurately estimate both  $T_c$  and  $T_s$  simultaneously, one of the translations must be discarded. Previous works [8] showed that, for the thigh, the magnitude of the STA is greater than the displacement of the joint center. Therefore, we decided to compute the best estimate of  $T_s$  and to assume that  $T_c$  is close to null. On the contrary, for the pelvis, it appears that the STA remains small. Thus, for this bone we assumed that  $T_s$  is close to null and we estimated  $T_c$  instead. In order to find the transformation (3 unknowns for the rotation in an axis-angle form and 3 for the translation) that minimizes the error made globally on the markers, the objective function to minimize for each segment and for each instant frame is as follows:

$$\sum_n (p_i - p'_i)^2 \quad (1)$$

with  $n$  the number of markers attached to the bone segment,  $p_i$  the recorded position of the  $i^{\text{th}}$  marker, and  $p'_i$  its estimated position. This is a least-squares minimization for which we used the rfsq optimizer [23]. Since the skin markers move nonlinearly [8], the solution converges faster thanks to the quadratic programming algorithm.

*Phase 2:* We assume that the position of the pelvis is correct, because the magnitude of the STA remains small for this bone. In case of collision between the articular bones, the position of the femur must be hence corrected, for each instant frame, in order to reach the non-penetrating state. This correction corresponds to a translation of the HJC of vector  $\mathbf{D}_{\text{HJC}}$  (**boldface** notation for vector). For fast computation, an uniform-level octree subdivision [17] is used for the hip bone model and the following algorithm is applied (see Fig. 3):

Let's consider  $\Phi$  being the *collider* (i.e., the femur) and  $\Gamma$  the *collided object* (i.e., the hip bone). The two meshes are defined by a set of points  $\Phi = \{P_i \in \mathbb{R}^3\}$  and  $\Gamma = \{Q_i \in \mathbb{R}^3\}$ , respectively. First, we project each point  $P_i$  onto  $\Gamma$ , yielding the projected point  $P_{i\perp}$ . Then,  $P_i$  is defined as being inside, and therefore colliding, if  $\mathbf{P}_i \mathbf{P}_{i\perp} \cdot \mathbf{N}_{\mathbf{P}_{i\perp}} > 0$  where  $\mathbf{N}_{\mathbf{P}_{i\perp}}$  is the outward normal at  $P_{i\perp}$ . This subset of  $k$  colliding points  $C_k = \{P_1, \dots, P_k\}$  creates the displacement vector:

$$\mathbf{D} = \frac{\sum_{i=1}^k \mathbf{P}_i \mathbf{P}_{i\perp}}{k} = \frac{\sum_{i=1}^k \mathbf{d}_i}{k} \quad (2)$$

The *collider* undergoes a translation proportional to the vector  $\mathbf{D}$ . This algorithm is iteratively performed for each instant frame, until no more collisions are detected. As a result, the translation  $\mathbf{D}_{\text{HJC}}$  of the HJC is equivalent to the sum of the translation vectors applied on the *collider*.

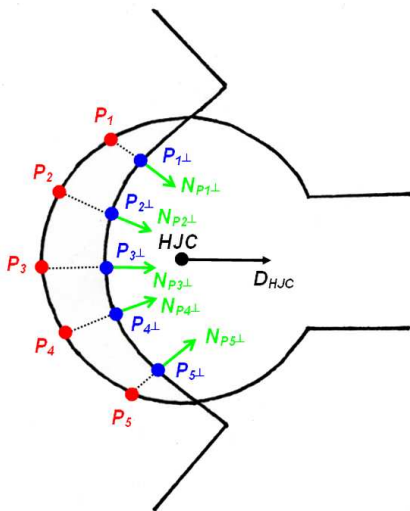


**Fig. 3** 2D schematic view of the collisions detection algorithm. The femur is corrected at each instant frame. As a result, the HJC undergoes a translation of vector  $\mathbf{D}_{HJC}$ .

*Validation:* The validation of the hip kinematics estimation was obtained using marker position data, collected during clinical motion patterns (flexion/ extension, abduction/ adduction, internal/ external rotation) on 6 volunteers scanned with a dynamic MRI protocol [16]. The subjects were equipped with external MRI-compatible marker sets and a tracking device was used to ensure the movements repeatability. For each instant frame, the position and orientation of both the hip and femur bones were computed and the kinematics derived from the marker position data were compared with that of the MRI bone tracking. Only the error on the femur translation/ orientation was calculated, since no markers were placed on the pelvis. Table 1 shows the femur position and orientation reconstruction errors expressed in the hip joint coordinates system.

As said previously in Sect. 2, the femur exhibits substantial skin motion. From these results, the STA errors for this bone are thus significantly reduced by the use of the proposed method.

**Table 1** Femur position X/Y/Z [mm] and orientation  $\alpha/\beta/\gamma$  [deg] reconstruction errors.

	X	Y	Z	$\alpha$	$\beta$	$\gamma$
Mean	0.45	0.19	0.37	3.28	1.49	0.43
RMS	0.59	0.24	0.4	3.86	1.71	0.55
Std	0.4	0.16	0.17	2.06	0.89	0.37

### 3.4 The simulation model

The base of this simulation model is a first-order finite-element system [4, 6, 11], which offers a good tradeoff between accuracy and computation speed in the context of soft tissues.

Since the only degrees of freedom of such models are the vertices of the mesh, it can be associated to any fast numerical integration method commonly used in particle systems [18], as well as good convenience for managing collisions, contacts and other geometrical constraints efficiently.

This model has been optimized to the context of large deformations through the corotational scheme: this avoids the nonlinearity of shear deformations by expressing the deformation state of the material in a local coordinate system oriented along the eigendirections of the strain tensor [20, 30]. This preserves accuracy in the linearized expression of the material strain, allowing linearity to offer a more robust processing of high compression states than the Saint-Venant-Kirchhoff models usually implemented in the context of large deformations [6, 19, 32].

We have associated this model to an adapted numerical integration scheme which uses either Newton-Raphson or Backward Euler steps, depending if static relaxation or dynamic simulation is used. Both take advantage of an efficient implementation of the Conjugate Gradient method which allows variable force Jacobian matrices to be accurately taken into account, key to an accurate processing of the nonlinearities resulting from large deformations.

This system provides us with a good performance in computing the strain and stress states of the deformable tissues, which can then be rendered interactively through adequate visualization techniques.

## 4 Results

### 4.1 Morphological analysis

Since our goal is to investigate idiopathic OA, we must first eliminate the typical abnormalities of the hip joint that could lead to cam/ pincer -FAI. Therefore, a morphological analysis is performed to evaluate the prevalence of the subject's hip joint. The morphology of the hip is well described by selected anatomical parameters.

One important parameter is the computation of the acetabular version which can be an indicator of pincer FAI [31]. We have implemented the standard measurement method from [33]. It is based on the angle between the sagittal direction and lines drawn between the anterior and posterior acetabular rim, at different heights (Fig. 4a). The angle is considered as positive when inclined medially to the sagittal plane (anteversion) and negative when inclined laterally to the sagittal plane (retroversion). Normal hips are anteverted.

Another indicator of pincer FAI is the acetabular depth [31]. The depth of the acetabulum is defined as the distance in mm between the center of the femoral head ( $O$ ) and the line  $AR - PR$  connecting the anterior ( $AR$ ) and posterior ( $PR$ ) acetabular rim (Fig. 4b). The value is considered as positive and normal if  $O$  is lateral to the line  $AR - PR$ .

Finally, a standard parameter related to the femur geometry is the femoral alpha ( $\alpha$ ) neck angle that is used for detecting cam FAI [31]. The  $\alpha$  angle is being defined by the an-



gle formed by the line  $O - O'$  connecting the center of the femoral head ( $O$ ) and the center of the femoral neck ( $O'$ ) at its narrowest point, and the line  $O - P$  connecting  $O$  and the point  $P$  where the distance between the bony contour of the femoral head and  $O$  exceeds the radius ( $r$ ) of the femoral head (Fig. 4c). Deviation from the normal geometry is usually associated with larger  $\alpha$  angles ( $> 60^\circ$ ). All the dancers' hips were analyzed, according to those 3 anatomical parameters. No morphological abnormalities were detected and it was concluded that all the measured hips were anteverted, with a positive depth and an  $\alpha$  angle in the normal range ( $30^\circ < \alpha < 55^\circ$ ). The results were validated by a radiological expert.

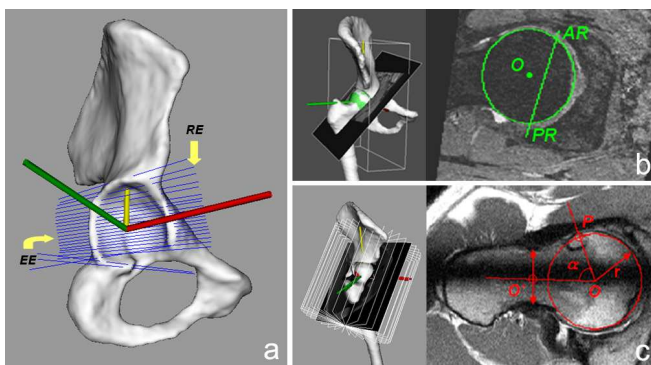


**Fig. 4** a) Computation of the acetabular version based on 3D reconstruction; roof edge ( $RE$ ) and equatorial edge ( $EE$ ) are lines drawn between the anterior and posterior acetabular edges, defining the orientation of the acetabular opening proximally and at the maximum diameter of the femoral head respectively (arrows) b) Definition of the acetabular depth (right) on a transverse oblique MR image (left) c) Definition of the  $\alpha$  angle (right) on a radial MR image (left), illustrating a cam type morphology ( $\alpha = 85^\circ$ ).

#### 4.2 Physical simulation

Simulation results are presented for one dancer. They were obtained during the simulation of the hip joint, where the labral deformations and pressures were computed. The elements present in our tests were: the hip and femur bones, as well as the tetrahedralized labrum. We investigated the three dancing's movements (grand pli , frontal split and d velopp    la seconde) recorded from the motion capture, as motion input. Since they all require extreme hip flexion and/or abduction, they should create significant stress in the articulation.

All the biomechanical materials considered in the current study were assumed as linear elastic and isotropic. The 3D models of the bones were hypothesized as rigid bodies, and the material properties for the labrum in terms of elastic modulus (Young's modulus  $E$ ) and Poisson's ratio ( $\nu$ ) were defined to be 20 MPa and 0.4, as depicted in [12]. The mechanical simulation first detects the collisions between the femur and labrum surfaces, using the previous

approach described in Sect. 3.3. Then, an appropriate collision response is computed, based on quadratic penalty forces [21]. The aim is to constrain the two models to reach the non-penetrating state.

We define the pressure  $P$  as the stress along the direction of the maximal compression. For each movement, the peak contact pressures of the labrum are plotted, as a function of motion (Fig. 5). Furthermore, Figure 6a shows for the three motions the pressure distribution within the labrum, for the instant frame where the maximal pressure was computed. Finally, Table 2 presents, for the three movements, the maximal and average peak pressures calculated during the entire motion, but only when collisions were detected.

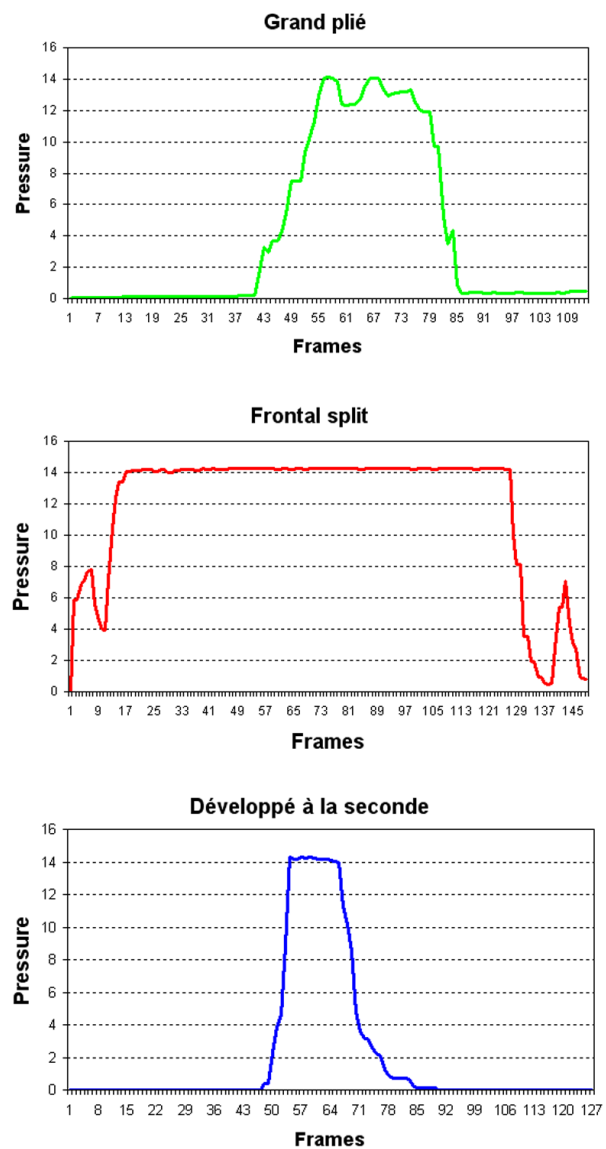


**Fig. 5** Peak contact pressures of the labrum during the whole motion.

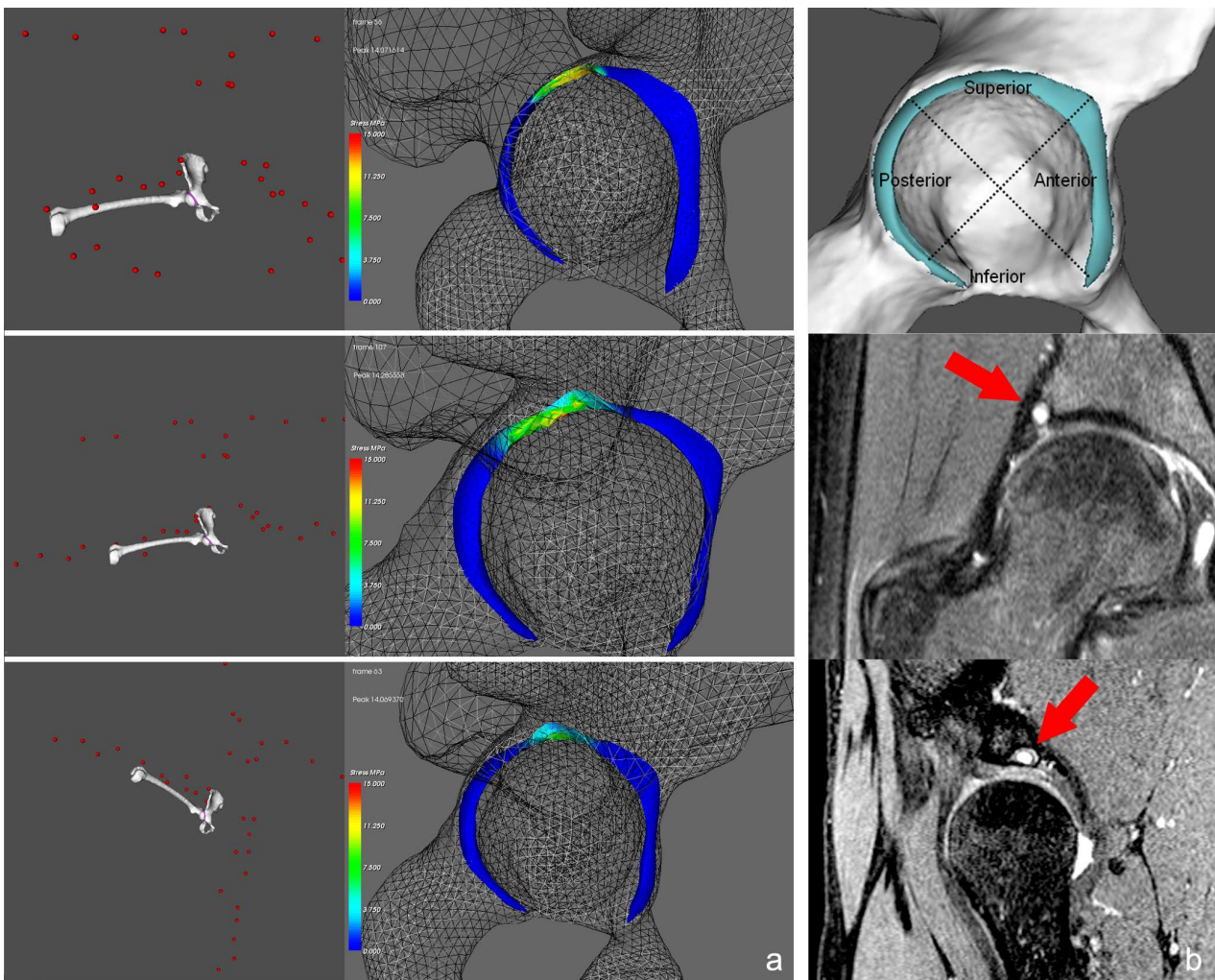


**Fig. 6** a) Computed motion and resulting pressure distribution within the labrum: grand pli  (top), frontal split (middle) and developp    la seconde (bottom). We clearly see that the maximal peak contact pressures occur at the maximal hip joint flexion and/or abduction b) Top: spatial partitioning of the acetabular region in quadrants. Middle and bottom: diagnosed labral lesions in patient's MR images (red arrows). The labral deformations (a) and the lesions (b) are both located in the superior quadrant of the acetabular rim.

**Table 2** Maximal and average peak pressures within the labrum, calculated during the entire motion, but only when collisions were detected.

Movement	Peak (MPa)	Mean (MPa)
Grand pli�	14.12	10.18
Frontal split	14.28	11.95
Developp� � la seconde	14.27	9.16

### 4.3 Interpretation

The subject's MR images were analyzed by a radiological expert. For the tested dancer, the localization of the labral lesions were diagnosed for both hips in the superior region of the acetabular rim. The labrum was considered as degenerated (abnormal signal intensity) for the left hip and torn (abnormal linear intensity extending to the labral surface) for the right hip. According to the three anatomical param-

eters, the morphological analysis for this subject reported an  $\alpha$  angle of  $42.95^\circ$  (left hip) and  $43.67^\circ$  (right hip), an acetabular depth of 8.06 mm (left hip) and 7.72 mm (right hip) and no retroversion. Thus, the subject's hips did not present any cam or pincer type morphology.

For the three movements analyzed, the maximal peak contact pressures occurred at maximal hip joint angle, as shown in Fig. 6a. Strong labral deformations were observed when the subject was performing extreme hip flexions or abductions. Moreover, the labral deformations were located in the superior area of the acetabular rim, which corresponds to the localization of diagnosed lesions (Fig. 6b). Finally, according to Table 2, the calculated maximal and average peak pressures are high compared to the normal situation. Indeed, previous studies [34] [10] reported cartilages pressures ranging from 2 MPa to 4 MPa for asymptomatic hips and daily activities. This corroborates the fact that the articulation undergoes a high stress during extreme hip motion. Moreover,

Fig. 5 reveals that such high pressures are often reached during dancing activities.

In conclusion, the simulation clearly demonstrates that both the pressure and its distribution within the labrum are clinically relevant with respect to radiologically observed damage zones in the labrum.

## 5 Discussion

In this paper, a methodology to perform functional simulations of the hip joint in extreme postures has been described. The use of optical motion capture allows us to accurately estimate bone poses of patient-specific hip joint, whereas the physical simulation provides us with accurate labral deformations and pressure indications in the simulated joint.

The simulation results have been reported for a single dancer, presenting no morphological abnormalities. These results already reveal that motion has a direct influence on the pressure distribution within the labrum. Moreover, a strong correlation is observed between the computed labral deformations and the diagnosed lesions. These are clinically encouraging results, but this methodology needs to be tested with additional subjects. However, there is little doubt that repetitive extreme hip motion could be a potential cause for the development of hip pain and OA in this selected population, with potential stigmata in the symptomatic dancers.

Future work will address the following points: The complex mechanical behavior of cartilage (i.e., non-linear and biphasic properties) will be considered. A more advanced simulation accounting for all the cartilages of the hip joint (labrum, acetabular and femoral cartilages) will also be investigated. Finally, further experiments will be carried out to estimate the error made on the hip kinematics during extreme movements, since currently only low amplitude motion was validated. For example, these experiments can be conducted in open MRI.

**Acknowledgements** This work is supported by the Co-Me project funded by Swiss National Research Foundation and by the FOCUS K3D project (FP7-ICT-2007-214993) funded by the European Union. We would like to thank the University Hospital of Geneva, Professor Pierre Hoffmeyer and Dr. Frank Kolo-Christophe, Etienne Lyard, Marlène Arévalo and Nedjma Cadi for their collaboration. We are also grateful to all volunteers from the ballet of the Great Theater of Geneva to have accepted to take part in the study.

## References

- Ahmet, C., Vahdet, U., Recep, K.: Three-dimensional anatomic finite element modelling of hemi-arthroplasty of human hip joint. *Trends Biomater Artif Organs* **21**, 63–72 (2007)
- Alexander, E., Andriacchi, T.: Correcting for deformation in skin-based marker systems. *J Biomech* **34**, 355–361 (2001)
- Assassi, L., Guillard, G., Gilles, B., Magnenat-Thalmann, N.: Volumetric meshes based on medial representation for medical applications. In: *Proc Comput Assist Orthop Surg (CAOS'07)*, pp. 259–262 (2007)
- Bathe, K.: *Finite element procedures*. Prentice Hall (1995)
- Benoit, D., Ramsey, D., Lamontagne, M., Xu, L., Wretenberg, P., Renstroem, P.: Effect of skin movement artifact on knee kinematics during gait and cutting motions measured in vivo. *Gait & Posture* **24**(2), 152–164 (2006)
- Bonet, J., Wood, R.: *Nonlinear continuum mechanics for finite element analysis*. Cambridge University Press (1997)
- Cappello, A., Cappozzo, A., Palombara, P.L., Lucchetti, L., Leardini, A.: Multiple anatomical landmark calibration for optimal bone pose estimation. *Hum Mov Sci* **16**(2–3), 259–274 (1997)
- Cappozzo, A., Catani, F., Leardini, A., Benedetti, M., Croce, U.D.: Position and orientation in space of bones during movement: experimental artefacts. *Clin Biomech* **11**(2), 90–100 (1996)
- Cereatti, A., Croce, U.D., Cappozzo, A.: Reconstruction of skeletal movement using skin markers: comparative assessment of bone pose estimators. *Journal of NeuroEngineering and Rehabilitation* **3**(7) (2006)
- Chegini, S., Beck, M., Fergusson, S.: Femoro acetabular impingement as a possible initiator of cartilage degeneration. In: *7th Int Symp on Comput Meth in Biomech and Biomed Eng (CMBBE2006)*, pp. 705–710 (2006)
- Cotin, S., Delingette, H., Ayache, N.: Real-time elastic deformations of soft tissues for surgery simulation. *IEEE Trans Visual Comput Graph* **5**(1), 62–73 (1999)
- Ferguson, S., Bryant, J., Ito, K.: The material properties of the bovine acetabular labrum. *J Orthop Res* **19**, 887–896 (2001)
- Ganz, R., Parvizi, J., Beck, M., Leunig, M., Notzli, H., Siebenrock, K.: Femoroacetabular impingement: a cause for osteoarthritis of the hip. *Clin Orthop Relat Res* **417**, 112–120 (2003)
- Gilles, B.: *Anatomical and kinematical modelling of the musculoskeletal system from mri*. Ph.D. thesis, Université de Genève (2007)
- Gilles, B., Moccozet, L., Magnenat-Thalmann, N.: Anatomical modelling of the musculoskeletal system from MRI. In: *Med Image Comput Comp Assist Intervention (MICCAI'06)*, pp. 289–296 (2006)
- Gilles, B., Perrin, R., Magnenat-Thalmann, N., Valle, J.P.: Bones motion analysis from dynamic MRI: acquisition and tracking. *Acad Radiol* **12**, 2385–2392 (2005)
- Gottschalk, S., Lin, M., Manocha, D.: Obbtree: A hierarchical structure for rapid interference detection. In: *SIGGRAPH'96*, pp. 171–180 (1996)
- Hauth, M., Etmuss, O.: A high performance solver for the animation of deformable objects using advanced numerical methods. In: *Eurographics'01*, pp. 137–151 (2001)
- Hauth, M., Gross, J., Strasser, W.: Interactive physically-based solid dynamics. In: *Eurographics Symp Comput Animation*, pp. 17–27 (2003)
- Hauth, M., Strasser, W.: Corotational simulation of deformable solids. In: *WSCG'04*, pp. 137–145 (2004)
- Hirota, G., Fisher, S., State, A., Lee, C., Fuchs, H.: An implicit finite element method for elastic solids in contact. In: *Comput Animation*, pp. 136–146 (2001)
- Kumagai, M., Kim, Y., Inoue, N., Genda, E., Liang, K.H.B., Koo, T., Chao, E.: 3-D dynamic hip contact pressure distribution in daily activities. In: *Summer Bioeng Conf*, pp. 53–54 (2003)
- Lawrence, C., Tits, A.: A computationally efficient feasible sequential quadratic programming algorithm. *SIAM J Optim* **11**(4), 1092–1118 (2001)
- Lewis, C., Sahrmann, S.: Acetabular labral tears. *Phys Ther* **86**, 110–121 (2006)
- Lu, T., O'Connor, J.: Bone position estimation from skin marker co-ordinates using global optimisation with joint constraints. *J Biomech* **32**, 129–134 (1999)
- Lucchetti, L., Cappozzo, A., Cappello, A., Croce, U.D.: Skin movement artefact assessment and compensation in the estimation of knee joint kinematics. *J Biomech* **31**(11), 977–984 (1998)
- Maciel, A., Sarni, S., Boulic, R., Thalmann, D.: Stress distribution visualization on pre- and post-operative virtual hip joint. In: *Proc Comp Assist Orthop Surg (CAOS'05)*, pp. 298–301 (2005)

28. Magnenat-Thalmann, N., Charbonnier, C., Schmid, J.: Multimedia application to the simulation of human musculoskeletal system: A visual lower limb model from multimodal captured data. In: Proc IEEE Int Workshop in Signal Processing, In Press (2008)
29. Manal, K., McClay, I., Richards, J., Galinat, B., Stanhope, S.: Knee moment profiles during walking: errors due to soft tissue movement of the shank and the influence of the reference coordinate system. *Gait & Posture* **15**, 10–17 (2002)
30. Nesme, M., Payan, Y., Faure, F.: Efficient, physically plausible finite elements. In: Eurographics'05, pp. 77–80 (2005)
31. Pfirrmann, C.W.A., Mengiardi, B., Dora, C., Kalberer, F., Zanetti, M., Hodler, J.: Cam and pincer femoroacetabular impingement: Characteristic mr arthrographic findings in 50 patients. *J Radiol* **240**(3), 778–785 (2006)
32. Picinbono, G., Delingette, H., Ayache, N.: Non-linear anisotropic elasticity for real-time surgery simulation. *Graph Model* **65**(5), 305–321 (2003)
33. Reynolds, D., Lucas, J., Klaue, K.: Retroversion of the acetabulum. a cause of hip pain. *J of Bone Joint Surgery* **81**(2), 281–288 (1999)
34. Russell, M., Shivanna, K., Grosland, N., Pedersen, D.: Cartilage contact pressure elevations in dysplastic hips: a chronic overload model. *J Orthop Surg Res* **1**(6), 169–177 (2006)
35. Schneider, P., Eberly, D.: Geometric tools for computer graphics. The Morgan Kaufmann Series in Computer Graphics and Geometric Modeling (2003)
36. Söderkvist, I., Biomech, P.W.J.: Determining the movements of the skeleton using well-configured markers. *J Biomech* **12**, 1473–1477 (1993)
37. Wu, G., Siegler, S., Allard, P., Kirtley, C., Leardini, A., Rosenbaum, D., Whittle, M., D'Lima, D., Cristofolini, L., Witte, H., Schmid, O., Stokes, I.: ISB recommendation on definitions of joint coordinate system of various joints for the reporting of human joint motion - part I: Ankle, hip and spine. *J Biomech* **35**(4), 543–548 (2002)